Advanced Functional Materials

Miniaturized battery-free wireless pulse oximeter system

--Manuscript Draft--

Manuscript Number:	adfm.201604373
Full Title:	Miniaturized battery-free wireless pulse oximeter system
Article Type:	Full Paper
Section/Category:	
Keywords:	NFC; oximetry; flexible electronics; wireless; photonics
Corresponding Author:	JEONGHYUN KIM University of Illinois at Urbana-Champaign Urbana, Illinois UNITED STATES
Additional Information:	
Question	**Response**
Please submit a plain text version of your cover letter here. **If you are submitting a revision of your manuscript, please do not overwrite your original cover letter. There is an opportunity for you to provide your responses to the reviewers later; please do not add them here**.	To the Editors: Please find the enclosed manuscript entitled Miniaturized Battery-free Wireless Pulse Oximeter System Jeonghyun Kim, Philipp Gutruf, Antonio M. Chiarelli, Seung Yun Heo, Kyoungyeon Cho, Zhaoqian Xie, Anthony Banks, Seungyoung Han, Kyung-In Jang, Jung Woo Lee, Kyu-Tae Lee, Yonggang Huang, Monica Fabiani, Gabriele Gratton, Ungyu Paik, and John A. Rogers*. We are submitting this work for consideration of publication in Advanced Functional Materials. This manuscript reports on materials and device concepts for ultraminiaturized wireless optoelectronic systems that incorporate advanced optoelectronic functionality for applications in wireless capture and transmission of photoplethysmograms, including quantitative information on blood oxygenation, heart rate and heart rate variability. Specifically, time-multiplexed reflectance pulse oximetry in conjunction with near-field communication (NFC) capabilities enables operation in thin, flexible devices with overall diameters of ~10 mm or less. Demonstrations of operation on various locations of the body and quantitative comparisons to clinical gold standards establish the versatility and the measurement accuracy of these systems and highlight advantages signal acquisition during operation under movement, respectively. The foundational science as well as the materials assembly techniques will be of broad interest to the readership of Advanced Functional Materials. We thank you in advance for your time and attention. Sincerely, John A. Rogers
Corresponding Author Secondary Information:	
Corresponding Author's Institution:	University of Illinois at Urbana-Champaign
Corresponding Author's Secondary Institution:	
First Author:	JEONGHYUN KIM
First Author Secondary Information:	
Order of Authors:	JEONGHYUN KIM
	Philipp Gutruf
	Antonio M. Chiarelli
	Seung Yun Heo
	Kyoungyeon Cho
	Zhaoqian Xie

	Anthony Banks
	Seungyoung Han
	Kyung-In Jang
	Jung Woo Lee
	Kyu-Tae Lee
	Xue Feng
	Yonggang Huang
	Monica Fabiani
	Gabriele Gratton
	Ungyu Paik
	John A. Rogers
Order of Authors Secondary Information:	
Abstract:	Development of unconventional technologies for wireless collection, storage and analysis of quantitative, clinically relevant information on physiological status is of growing interest. Soft, biocompatible systems are widely regarded as important because they facilitate mounting on external (e.g. skin) and internal (e.g. heart, brain) surfaces of the body. Ultra-miniaturized, lightweight and battery-free devices have the potential to establish complementary options in bio-integration, where chronic interfaces (i.e. months) are possible on hard surfaces such as the fingernails and the teeth, with negligible risk for irritation or discomfort. Here we report materials and device concepts for flexible platforms that incorporate advanced optoelectronic functionality for applications in wireless capture and transmission of photoplethysmograms, including quantitative information on blood oxygenation, heart rate and heart rate variability. Specifically, reflectance pulse oximetry in conjunction with near-field communication (NFC) capabilities enables operation in thin, miniaturized flexible devices. Studies of the material aspects associated with the body interface, together with investigations of the radio frequency characteristics, the optoelectronic data acquisition approaches and the analysis methods capture all of the relevant engineering considerations. Demonstrations of operation on various locations of the body and quantitative comparisons to clinical gold standards establish the versatility and the measurement accuracy of these systems, respectively.

DOI: 10.1002/ ((please add manuscript number))
Article type: Full Paper

Miniaturized battery-free wireless pulse oximeter system

*Jeonghyun Kim[†], Philipp Gutruf[†], Antonio M. Chiarelli, Seung Yun Heo, Kyoungyeon Cho, Zhaoqian Xie, Anthony Banks, Seungyoung Han, Kyung-In Jang, Jung Woo Lee, Kyu-Tae Lee, Xue Feng, Yonggang Huang, Monica Fabiani, Gabriele Gratton, Ungyu Paik, and John A. Rogers**

[*] Prof. J. A. Rogers, Corresponding author
Departments of Materials Science and Engineering, Biomedical Engineering, Chemistry, Neurological Surgery, Mechanical Engineering, Electrical Engineering and Computer Science
Simpson Querrey Institute & Feinberg Medical School
Center for Bio-Integrated Electronics
Northwestern University
Evanston, IL 60208, USA
E-mail: jrogers@northwestern.edu

Dr. J. Kim, Dr. P. Gutruf, S. Y. Heo, A. Banks, Dr. S. Han, Dr. K.-I. Jang, Dr. J. W. Lee, Dr. K.-T. Lee, Prof. J. A. Rogers
Department of Materials Science and Engineering
Frederick Seitz Materials Research Laboratory
University of Illinois at Urbana-Champaign
Urbana, IL 61801, USA

Dr. P. Gutruf, Dr. K.-T. Lee
Departments of Materials Science and Engineering
Northwestern University
Evanston, IL 60208, USA

Dr. A. M. Chiarelli, Prof. M. Fabiani, Prof. G. Gratton
Beckman Institute
University of Illinois at Urbana-Champaign
Urbana, IL 61801, USA

S. Y. Heo
Departments of Biomedical Engineering
Northwestern University
Evanston, IL 60208, USA

K. Cho
Department of Electrical and Computer Engineering
Frederick Seitz Materials Research Laboratory
University of Illinois at Urbana-Champaign
Urbana, IL 61801, USA

Dr. Z. Xie
Department of Civil and Environmental Engineering
Northwestern University
Evanston, IL 60208, USA

Prof. X. Feng
AML, Department of Engineering Mechanics
Center for Mechanics and Materials
Tsinghua University, Beijing 100084, China

Prof. Y. Huang
Departments of Civil and Environmental Engineering, Mechanical Engineering, Materials Science and Engineering
Center for Engineering and Health, and Skin Disease Research Center
Northwestern University
Evanston, IL 60208, USA

Prof. U. Paik
Department of Energy Engineering
Hanyang University
Seoul, 133-791, Republic of Korea

[†] These authors contributed equally to this work.

Keywords: NFC, oximetry, flexible electronics, wireless, photonics

Abstract

Development of unconventional technologies for wireless collection, storage and analysis of quantitative, clinically relevant information on physiological status is of growing interest. Soft, biocompatible systems are widely regarded as important because they facilitate mounting on external (e.g. skin) and internal (e.g. heart, brain) surfaces of the body. Ultra-miniaturized, lightweight and battery-free devices have the potential to establish complementary options in bio-integration, where chronic interfaces (i.e. months) are possible on hard surfaces such as the fingernails and the teeth, with negligible risk for irritation or discomfort. Here we report materials and device concepts for flexible platforms that incorporate advanced optoelectronic functionality for applications in wireless capture and transmission of photoplethysmograms, including quantitative information on blood oxygenation, heart rate and heart rate variability. Specifically, reflectance pulse oximetry in conjunction with near-field communication (NFC) capabilities enables operation in thin, miniaturized flexible devices. Studies of the material aspects associated with the body interface, together with investigations of the radio frequency characteristics, the optoelectronic data acquisition approaches and the analysis methods capture all of the relevant engineering considerations. Demonstrations of operation on various locations of the body and quantitative comparisons to clinical gold standards establish the versatility and the measurement accuracy of these systems, respectively.

1. Introduction

The growing interest in advanced body-worn electronic/optoelectronic systems for health monitoring applications is evidenced both by the rapid proliferation of research articles in the scientific literature and by the expanding collection of devices availaible on the consumer and clinical markets[1, 2]. A strong development trend involves technologies that expand beyond qualitative measurements (e.g. activity levels, or 'steps') toward quantitative sensing with direct correlates to clinical gold standards, and an emphasis on continuous monitoring of all vital signs. An intimate, long-lived, comfortable and non-irritating interface to the body is critical for this purpose. Soft, skin-like systems, sometimes referred to as 'epidermal electronics'[3], offer attractive characteristics in this context, with many published examples of sensing functionality in support of recently launched commercial products[4]. A recently reported, complementary strategy focuses on device miniaturization rather than soft mechanics, where surfaces such as those of the fingernails, instead of the skin, form the point of integration and the measurement interface[5]. The mechanical rigidity of the fingernails/toenails, the absence of nerve endings and minimal interfacial water loss make this body location attractive as a point for long-term device integration. The optical transparency can be exploited as a window for capturing time-dynamic spectral information on properties of blood in the underlying capillary beds. Amongst the most popular measurements of this general type is pulse oximetry[6] and photoplethysmography, due to the clinically established relevance of these data in assessments of cardiovascular health. Here, light emitted in the red and infrared can backscatter from or transmit through the tissue for measurement of pulsatile variations in hemoglobin concentration, thereby allowing calculation of arterial oxygen saturation, heart rate, heart rate variability and other key parameters related to the cardiac pulse[1, 6, 7].

Particularly for reflectance based oximetry systems, severe motion artifacts result from slight, unintentional variations in optical path associated with normal body movements[8]. Such

phenomena, together with the need for bulky hardware, often with wired approaches to data transfer and/or batteries for power supply, represent significant disadvantages for even the most advanced wearable oximeters that are currently available. An attractive alternative approach exploits thin, conformal skin-mounted measurement platforms that exploit NFC technology to supply sufficient power to operate light emitting diodes, photodetector and signal conditioning electronics[2] and to wirelessly transmit data with sufficient bandwidths[4]. Motion artifacts can, however, still be significant and long-term integration on the skin can, in some cases, disrupt natural patterns of transepidermal water loss, cause irritation at the skin interface and involve time-dependent degradations in adhesion due to the gradual accumulation of exfoliated dead cells at the surface of the stratum corneum.

In this work we introduce an alternative approach that focuses on device miniaturization, in thin flexible forms that can be mounted on nearly any location of the body, including the fingernails/toenails. The key advances over previously reported skin-mounted systems with related functionality are in a millimeter-scale bilayer loop antenna design for improved inductance and an electronic system built around a microcontroller, instad of an astable multivibrator circuit, for precise control over the operation of the optoelectronic components and the relative timing accuracy. The result is a complete functional system at a size scale of ~10 mm in diameter, with a thickness of ~0.9 mm, a flexural rigidity of 8.7×10^{-2} N m, and a degree of bendability to a radius of 3 mm in curvature. Overall weight and areal size of these millimeter-scale wireless systems are significantly (10X and 13X) smaller than previous, skin-mounted devices. The result is an unusual optical measurement platform that can be directly interfaced to the body and, for the case of the fingernail, can support operation continuously for up to 3 months without risk for irritation, discomfort or device degradation limited only by the growth rate of the fingernails.

2. Results and Discussion

The technology builds on NFC electronic systems recently reported in epidermal formats for data storage, UV sensing and optical characterization of the skin[2]. Levels of miniaturization needed for fingernail embodiments require rigorous size miniaturization of the antenna structures (by 13X), reduction of the number of active and passive components (from 22 to 12) and increases in the density of integration (from 32% to 63% in area coverage of active and passive components). The latter aspect is particularly powerful because considerations in layouts for soft, biocompatible mechanics because miniaturized platforms such as those introduced here bypass requirements in designs for stretechability. Specifically, the architecture exploits a multilayer layout with a bilayer loop antenna configured to maximize the efficiency for energy harvesting and the distance for wireless data communication, as in Figure 1A. A dual layer interconnect matrix on a thin substrate affords compact electrical routing between closely spaced components. A soft opaque material, namely a silicone elastomer (Q1-4010, Dow Corning) with a black dye (5 wt%), with openings for the optical components coats the surface of this thin, flexible system (Figure S1), to facilitate conformal contact with the target probing area (i.e. fingernail, toenail or various skin locations) and to provide protection against mechanical damage.

Integrated functions available in an NFC bare die chip (SL13A, AMS AG) allow significant reductions in the number of components, compared to previously reported systems. As in the simplified schematic illustration of Figure 1B, this chip provides harvests wirelessly delivered power for operation of a microcontroller and an operational amplifier. The microcontroller drives infrared and red LEDs in a time sequenced manner. An integrated photodetector positioned in between these two LEDs captures the backscattered light. An analog to digital converter in the NFC chip amplifies and digitizes the resulting signal, and then transmits the information wirelessly via an integrated data management function.

The distance between LEDs and the photodetector[9], namely the inter-optode distance, has a strong influence on the signal to noise ratio. The layout presented here places the photodetector equidistant between the red and IR light sources, with minimum separation to allow adequate data collection capabilities. Generally, in reflectance systems, increasing the distance enhances the variations in signal associated with pulsatile blood flow, simply to the a corresponding increase in the effective probing volume[10]. This increased distance exponentially decreases, however, the amount of light that can be detected. These considerations, together with constraints on the overall device size, lead us to select a distance of 2 mm. In this geometry, the measurements yield excellent data quality, in terms of signal to noise, with a size that remains compatible with the main location of interest for integration, the fingernails/toenails.

As shown in Figure 1C, the resulting layout efficiently uses the available space. An encapsulated device operating next to a US penny appears in Figure 1D. This miniaturization allows for the integration on a fingernail, as demonstrated in Figure 1E. As shown in Figure 1F, the red and infrared LEDs have narrowband spectral output centered at 625 nm and 950 nm. Video S1 and Figure 1G show an operating device and time-multiplexed outputs from the photodetector. The LEDs operate at current levels selected to allow high gain amplification of the photodetector response, and therefore improved signal to noise performance. The resulting raw output of the photodiode obtained wirelessly is displayed in Figure 1H. The pulsatile component associated with blood flow appears clearly in the time multiplexed envelope of the signal.

Such flexible, miniaturized devices provide advantages in mechanics for mounting on the skin and the nail, due directly to their small size as outlined in quantitative detail in the context of previously reported, simple systems with similar form factors. In particular, the small size minimizes sensory perception and reduces energy release rates for delamination[5]. The

devices can also accommodate bending without significant change in performance. This tolerance to bending follows from a design that locates the electronic components near the mechanical neutral plane, in the middle of the black encapsulation layer (Figure S2). The image in Figure 2A shows a device bent to a small radius of curvature, as a highlight of this mechanical robustness. The mechanical properties of the encapsulation layer are important because this material defines the contacting interface. Figure 2B shows the stress-strain curves of various types of encapsulation layers. The low moduli of these materials enable conformal contact with the body and can be selected, independent of the electronics, to match the properties of the target mounting location. A biocompatible adhesive (PC2723U, ScapaHealthcare, UK) bonds the device to the body. Figure 2C shows results from mechanical measurements obtained using a T-peeling tester equipped with a high-resolution force gauge (Mark-10, Copiague, NY, Resolution: ± 0.25%, standard ISO 29862:2007) on devices mounted on the fingernail (black line) and the skin (red line). The measurement set-up and method are shown in Figure S3. The adhesive ensures strong adhesion to both the fingernail nail (~9.4 kPa) and the skin (~7.9 kPa). The low modulus (~17 kPa) of the encapsulation layer and the strong adhesion provide a stable and robust mounting which can eliminate the movement artifacts. The device can function properly even under movement, because of the stable interface (Video S2). The performance is excellent in both flat and bent geometries, as determined by operation while mount on planar and curved substrates (Figure 2D and E), the latter of which has a 5 mm radious of curvature, comparable to the minimum curvature of fingernails in adults[11]. The RF properties, as evidenced by the phase response, do not depend strongly on curvature in this range, shown in Figure 2F. aAn additional point of interest is that the devices can operate when submerged in water, as in Figure S4.

Figure 3 displays the results of oximeter measurements performed on a fingernail. Figure 3A shows signals recorded for 10 seconds during a 30 seconds resting period. Figure 3A, from top to bottom, presents the photodetector response associated with the infrared and red wavelengths, the extracted heart rate (HR), expressed in beats per minute (BPM), the R value and the SpO_2 level. Descriptions of computational procedures are in the analysis section. Test that involve holding of one's breath for 70 seconds (shaded areas) during data collection with both a fingernail device and a reference commercial system (IHealth, Apple inc.) on the same subject provides a dynamic SpO_2 level estimate comparison of the two systems. The results indicate a change in SpO_2 level within a range of ~87-98 %. From left to right, the graphs summarize the R value (Figure 3B) and the SpO_2 level (Figure 3C) from the fingernail device, and the SpO_2 level from the commercial system (Figure 3D). For the fingernail device, the equation that links the R value and SpO_2 follows from the modified Lambert-Beer equation as outlined in the Experimental section. The resulting SpO_2 levels show behaviors that agree quantitatively with the commercial system for breath hold tests across multiple subjects. In other words, the system is usable across subjects without the need for recalibration. Table 1 shows the average SpO_2 values and standard deviations for measurements conducted continuously for ~1 min on six different subjects, each in a state of rest. The SpO_2 values are all near 99 % and the standard deviations are under 1.5 which is an excellent result for an oximetry system when compared to even more elaborate state of the art systems, which generally provide a 2-3% tolerance on SpO_2 estimation. All other data are shown in Table S1.

Additional studies highlight the unique nature of measurements using this type of platform deployed on a fingernail/toenail. Figure 4A shows the extraction of the SpO_2 from a subject during a 15 seconds period of no movement followed by a 30 seconds period of movement of the finger and 15 seconds period of no movement. Simultaneously recordings from an

accelerometer affixed to the finger quantify the movements. The stable extraction of the SpO_2 value during movement highlights advantages of such a miniaturized concept especially for chronically ill subjects with involuntary hand movements. We highlighted the signal stability by drawing a direct comparison to a commercially available oximetry system in the supplementary information Figure S4. To further emphasize unique advantages, especially those that follow from possibilities for mounting on the fingernail, we compared to results obtained with a commercial reflectance based system mounted on the wrist, the prevalent location adapted in smart watches and fitness trackers. Data recording occurred over a period of 20 seconds with the arm held completely still as indicated in the accelerometer graphs in Figure S5. In the marked area, the fingers of the arm where moved, causing a slight change of the underling probing volume due to the activation of the extensor digitorum and extensor indicis. These changes result in significant distortions of the signal seen in Figure S5, making the extraction pulse and SpO_2 impossible during activities such as typing on a keyboard. With the systems presented here, such distortions are minimal due to the absence of relative motion between the device, the fingernail and the underlying soft tissue.

The ultraminiaturized form and the wireless functionality also enable the device to be used in a diverse range of scenarios. As examples, similar measurements are possible on a fingernail and an earlobe. In the latter case, a computer mouse can be equipped with NFC reader capabilities, allowing for continuous, or nearly continuous, measurements during use of the computer, as in Figure 4B. Also, smartphones and tablets can be potential platforms for continuous monitoring during common daily activities because of their frequent use. Figure 4C and D show the extracted photodetector signals and the SpO_2 level, respectively, captured from a device mounted on the fingernail. The full data set is in Figure S6. In the former case, i.e. the back of an earlobe, an NFC interface in a smartphone can enable data collection during phone calls as shown in Figure 4E. Figure 4F and G show data captured in this mode. This

hard to reach mounting location, not usually accessible with current conventional systems, also provides discretion for a long term measurement as the oximeter is not easily visible. The full data set is in Figure S7.

3. Conclusion

The results reported here provide the foundations for millimeter-scale, battery-free optoelectronic systems capable of wirelessly capturing photoplethysmograms and quantitative information on blood oxygenation, heart rate and heart rate variability. When implemented with a soft, optically opaque encapsulation material, the systems are thin, lightweight and mechanically compliant, thereby providing great versatility in choice of mounting location. Operation on the fingernail, in particular, is highly desirable for long term operation, with minimized motion artifacts and risks for irritation. Extensions of this platform should allow additional modes of operation with relevance to clinical medicine and human health.

4. Experimental Section

Device fabrication

Fabrication of the coils involved photolithography and wet etching to define traces on both sides of a Cu (18 μm) / PI (12 μm) / Cu (18 μm) foil. Via connections for the circuit and the coil were formed by electroplating through corresponding holes, defined lithographically. After removal of native oxide layers, a thinned NFC bare die (SL13A, AMS AG, 100 μm) with Au ball-bumps to enhance solderability and other electrical components was attached to the Cu traces with an In/Ag soldering paste (Ind. 290, Indium Corporation). The encapsulation layer consisted of a silicone elastomer (Q1-4010, Dow Corning) with a black dye (5 wt%).

Components

The critical components are as follows:

NFC (SL13A, AMS AG, 2.36 mm x 2.36 mm x 0.1 mm)

Microcontroller (ATtiny10, Atmel, 2 mm x 2 mm x 0.6 mm)

Amplifier (ADA 4505-2, Analog Devices, Inc, 1.42 mm x 1.42 mm x 0.6 mm)

IR LED (SFH 4043, 950 nm, Osram Opto Semiconductor, 1 mm x 0.5 mm x 0.45 mm)

Red LED (LR QH9F, 625 nm, Osram Opto Semiconductor, 1 mm x 0.5 mm x 0.35 mm)

Photodetector (EMD7000X01, Vishay Semiconductors, 2 mm x 1.25 mm x 0.85 mm)

Programming

Programming of the microcontroller (ATTiny10) emphasized low power operation and accurate time management. The code was written in C programming language and was compiled using Atmel studio7. The microcontroller was programmed using an Atmel ICE JTAG programming system before system assembly.

Pulse oximeter in vivo measurements

The wireless pulse oximeter was tested on human subjects and compared to a commercial system (IHealth, Apple inc.). The device reported here uses reflection mode and it was placed on the middle finger tip. The commercial transmittance system was placed on the index finger tip. Both systems were placed on the subjects' right hand. Arterial oxygen saturation was determined over a measurement period of 30 seconds on four subjects, each at rest. A breath holding task was performed for purposes of comparison over a range of saturation levels. (85%-98%)

Additional measurements involved mounting on the fingertip, fingernail and earlobe of one participant.

Pulse Oximeter data analysis

The Pulse Oximeter data analysis was performed off-line using a commercial software package (MATLAB R2013b, The MathWorks Inc.). The data collection involved a sampling rate of

25 Hz, with characteristic alternating output levels corresponding to switching between the two LEDs (12 Hz, Red: 640 nm, InfraRed: 950 nm). These levels were extracted using a local minima-maxima finding algorithm. This procedure provided a sampling rate of 6 Hz for each wavelength. Resulting time dependent variations in signal were reconstructed by spline interpolation of the sampled points[12]. Each wavelength signal was bandpass filtered (0.5-3 Hz, 10th order Butterworth digital filter) to extract the pulsating component (AC(t)) and low-pass filtered (0.2 Hz, 10th order Butterworth digital filter) to extract the slow signal component unrelated to pulsation (DC(t)). The relative pulsatile signal intensity S(t) was computed as the ratio of the two signals for both the red and the infrared wavelengths.

$$S(t) = \frac{AC(t)}{DC(t)} \quad (1)$$

The ratio R(t) between the red and infrared pulsatile components[13] was computed every second over an integration time window of 5 seconds as:

$$R(t) = \frac{\ln(rms(S(T)_R)+1)}{\ln(rms(S(T)_{IR})+1)} \quad (2)$$

for T from t-2.5s to t+2.5 s, where ln is the natural logarithm operator, rms is the root mean square operator and $S(t)_R$ and $S(t)_{IR}$ are the red and infrared relative pulsatile signal respectively.

From photon-diffusion analysis and the modified Lambert-Beer equation[14], the following equation can be derived for the relationship between the arterial blood saturation SpO_2 and the R(t) value[15]:

$$SpO2(t) = \frac{\varepsilon_{Hb}(\lambda_R)DPF_{R-IR} - \varepsilon_{Hb}(\lambda_{IR})R(t)}{[\varepsilon_{Hb}(\lambda_R) - \varepsilon_{HbO_2}(\lambda_R)]DPF_{R-IR} + [\varepsilon_{HbO_2}(\lambda_{IR}) - \varepsilon_{Hb}(\lambda_{IR})]R(t)} \quad (3)$$

Where $\varepsilon_{HbO_2}(\lambda_R)$ and $\varepsilon_{Hb}(\lambda_R)$ are the extinction coefficients of oxy- and deoxy-hemoglobin for red light (wavelength of 640 nm) and $\varepsilon_{HbO_2}(\lambda_{IR})$ and $\varepsilon_{Hb}(\lambda_{IR})$ are the extinction coefficients of oxy- and deoxy-hemoglobin for infrared light (wavelength of 950

nm). The extinction coefficients of the two forms of hemoglobin at the two wavelengths were extracted from[16], ($\varepsilon_{HbO_2}(\lambda_R)$ = 0.011 mm^{-1}, $\varepsilon_{Hb}(\lambda_R)$ = 0.106 mm^{-1}, $\varepsilon_{HbO_2}(\lambda_{IR})$= 0.028 mm^{-1}, $\varepsilon_{Hb}(\lambda_{IR})$ = 0.018 mm^{-1}). The quantity DPF_{R-IR} describes the effects of the dissimilar optical path lengths at the two wavelengths and can be expressed as the ratio of the Differential Pathlength Factors[17] (DPFs) of the red and infrared lights $DPF_{R-IR} = {DPF_R}/{DPF_{IR}}$. The color dependence of the optical pathlength depends on the scattering nature of the biological tissue and its dependence on the light wavelength. If DPF_{R-IR} is considered equal to 1, equation 3 is identical to the one derived using the simple Lambert-Beer law. This approximation, however, provides a poor estimate of SpO_2. A practical problem when using equation 3 for SpO_2 estimation is that DPF_{R-IR} depends on the baseline optical properties of the tissue (namely reduced scattering coefficient and absorption coefficient at the two wavelengths), and thus on tissue micro-structure and, importantly, on SpO_2 itself[18]. This issue is generally overcome by calibrating the oximeter empirically. If the range of saturation value is small (80%-100%), a constant DPF_{R-IR} can be considered. Based on literature and empirical results from our measurements, we set the DPF_{R-IR} to $DPF_{R-IR} = 1.4$[18, 19]. This value accounted for the increased optical path length of red light compared to infra-red light. Equation 1 yielded arterial oxygen saturation levels close the one reported by the commercial system on different subjects and in the range of saturation investigated (85%-100%). A different calibration curve might be needed (one in which DPF_{R-IR} is not considered constant) for measurements over an expanded range of saturation values. In this paper, an extracted Beat Per Minute (BPM) signal BPM(t) is reported for some data. The time dependence of BPM was estimated as:

$$BPM(t) = 60f(t)_{max-IR} \quad (4)$$

Where $f(t)_{max-IR}$ was the frequency at which $\|fft(S(T)_{IR})\|$ presented its maximum for T from t-2.5s to t+2.5 s. fft is the fast fourier transform operator.

Supporting Information

Supporting Information is available from the Wiley Online Library or from the author.

Acknowledgements

J. Kim and P. Gutruf contributed equally to this work. This work was supported by funding from the SQI Center for Bio-Integrated Electronics, and used facilities in the Frederick Seitz Materials Research Laboratory and the Center for Microanalysis of Materials at the University of Illinois at Urbana-Champaign. Z.X. and X.F. acknowledge the support from the National Basic Research Program of China (Grant No. 2015CB351900) and National Natural Science Foundation of China (Grant Nos.11402134, 11320101001). Y.H. acknowledges the support from NSF (Grant Nos. DMR-1121262, CMMI-1300846, CMMI-1400169 and 1534120) and the NIH (Grant No. R01EB019337)

Received: ((will be filled in by the editorial staff))
Revised: ((will be filled in by the editorial staff))
Published online: ((will be filled in by the editorial staff))

References

[1] T. Yokota, P. Zalar, M. Kaltenbrunner, H. Jinno, N. Matsuhisa, H. Kitanosako, Y. Tachibana, W. Yukita, M. Koizumi, T. Someya, Science advances 2016, 2, e1501856; C. M. Lochner, Y. Khan, A. Pierre, A. C. Arias, Nature Communications 2014, 5, 5745.

[2] J. Kim, G. A. Salvatore, H. Araki, A. M. Chiarelli, Z. Xie, A. Banks, X. Sheng, Y. Liu, J. W. Lee, K.-I. Jang, S. Y. Heo, K. Cho, H. Luo, B. Zimmerman, J. Kim, L. Yan, X. Feng, S. Xu, M. Fabiani, G. Gratton, Y. Huang, U. Paik, J. A. Rogers, Science Advances 2016, 2, e1600418.

[3] D. H. Kim, N. S. Lu, R. Ma, Y. S. Kim, R. H. Kim, S. D. Wang, J. Wu, S. M. Won, H. Tao, A. Islam, K. J. Yu, T. I. Kim, R. Chowdhury, M. Ying, L. Z. Xu, M. Li, H. J. Chung, H. Keum, M. McCormick, P. Liu, Y. W. Zhang, F. G. Omenetto, Y. G. Huang, T. Coleman, J. A. Rogers, Science 2011, 333, 838.

[4] J. Kim, A. Banks, H. Cheng, Z. Xie, S. Xu, K. I. Jang, J. W. Lee, Z. Liu, P. Gutruf, X. Huang, P. Wei, F. Liu, K. Li, M. Dalal, R. Ghaffari, X. Feng, Y. Huang, S. Gupta, U. Paik, J. A. Rogers, Small 2015, 11, 906.

[5] J. Kim, A. Banks, Z. Xie, S. Y. Heo, P. Gutruf, J. W. Lee, S. Xu, K. I. Jang, F. Liu, G. Brown, J. Choi, J. H. Kim, X. Feng, Y. Huang, U. Paik, J. A. Rogers, Advanced Functional Materials 2015, 25, 4761.

[6] K. K. Tremper, Chest Journal 1989, 95, 713.

[7] J. E. Sinex, The American journal of emergency medicine 1999, 17, 59.

[8] Y.-S. Yan, Y.-T. Zhang, IEEE Transactions on information technology in biomedicine 2008, 12, 399.

[9] J. L. Reuss, IEEE transactions on biomedical engineering 2005, 52, 153.

[10] Y. Mendelson, B. D. Ochs, IEEE Transactions on Biomedical Engineering 1988, 35, 798.

[11] S. Murdan, International journal of cosmetic science 2011, 33, 509.

[12] C. De Boor, C. De Boor, E.-U. Mathématicien, C. De Boor, C. De Boor, *A practical guide to splines*, Vol. 27, Springer-Verlag New York, 1978.

[13] J. P. Dekock, L. Tarassenko, Medical & Biological Engineering & Computing 1993, 31, 291.

[14] A. Sassaroli, S. Fantini, Physics in Medicine and Biology 2004, 49, N255.

[15] J. M. Schmitt, Ieee Transactions on Biomedical Engineering 1991, 38, 1194; D. R. Tobler, M. K. Diab, R. J. Kopotic, U.S. Patent No. 6,285,896, 2001.

[16] W. Zijlstra, A. Buursma, W. Meeuwsen-Van der Roest, Clinical chemistry 1991, 37, 1633.

[17] F. Fabbri, A. Sassaroli, M. E. Henry, S. Fantini, Physics in medicine and biology 2004, 49, 1183.

[18] J. Kohl, G. Noci, E. Antonucci, G. Tondello, M. Huber, S. Cranmer, L. Strachan, A. Panasyuk, L. Gardner, M. Romoli, The Astrophysical Journal Letters 1998, 501, L127.

[19] F. Scholkmann, U. Gerber, M. Wolf, U. Wolf, Neuroimage 2013, 66, 71.

Figure captions

Figure 1. (A) Exploded-view schematic illustration of the various constituent layers of a millimeter-scale, NFC enabled pulse oximeter device. (B) Block diagram of the functional components. (C) Image of an unencapsulated device. (D) Image of an encapsulated device, next to a US one cent coin. (E) Image of adevice during operation while mounted on a thumbnail. (F) Emission spectrum of the infrared and red light emitting diodes used in these devices. (G) Time-resolved current applied to the red and infrared light sources. (H) Wirelessly obtained data corresponding to the the amplified photodetector signal.

Figure 2. (A) Image of the device bent to a small radius of curvature with a pair of tweezers. (B) Stress-strain curves of opaque encapsulation layers with various materials. (C) Adhesion force measurements performed on encapsulation layers adhered to the nail and the skin. (Peel rate: 50 μm/s). Demonstrations of conformal contact with (D) a flat surface and (E) a curved surface. (F) Phase responses associated with the flat and curved devices.

Figure 3 (A) SpO_2 calculation from raw signal obtained from the device on the fingertip. Extracted IR signal. Extracted Red signal. Relative values of Red and IR signals. Extracted heart rate, in beats per minute (bpm). Calculated ratio of red and IR signal (R-ratio). Calculated SpO_2. (B) R ratio recorded during a breath hold test. The results how the expected physiological changes. (C) Calculated SpO_2 during breath hold test showing a visible drop in oxygen saturation. (D) Data from a commercial oximeter (IHealth, Apple inc.) simultaneously worn during breath hold test, as a reference. The shaded areas indicate periods of breath holding.

Figure 4. Demonstration of device operation during movement and on various body locations. (A) Calculated SpO_2 during periods of 15 s of rest, 30 s of movement, and 15 s of rest. The movement is quantified by the output of a X, Y, Z-axis accelerometer. (B) Demonstration of a possible application on a computer input device. (C) Relative values of Red and IR signal obtained from mounting on the fingernail. (D) Calculated SpO_2 from the fingernail. (E) Demonstration of mounting on the back of the earlobe. The inset shows the front of the earlobe during the device operation. (F) Relative values of Red and IR signal obtained from the earlobe. (G) Calculated SpO_2 from the earlobe.

Table 1. Mean and standard deviations of calculated SpO_2 for multiple subjects.

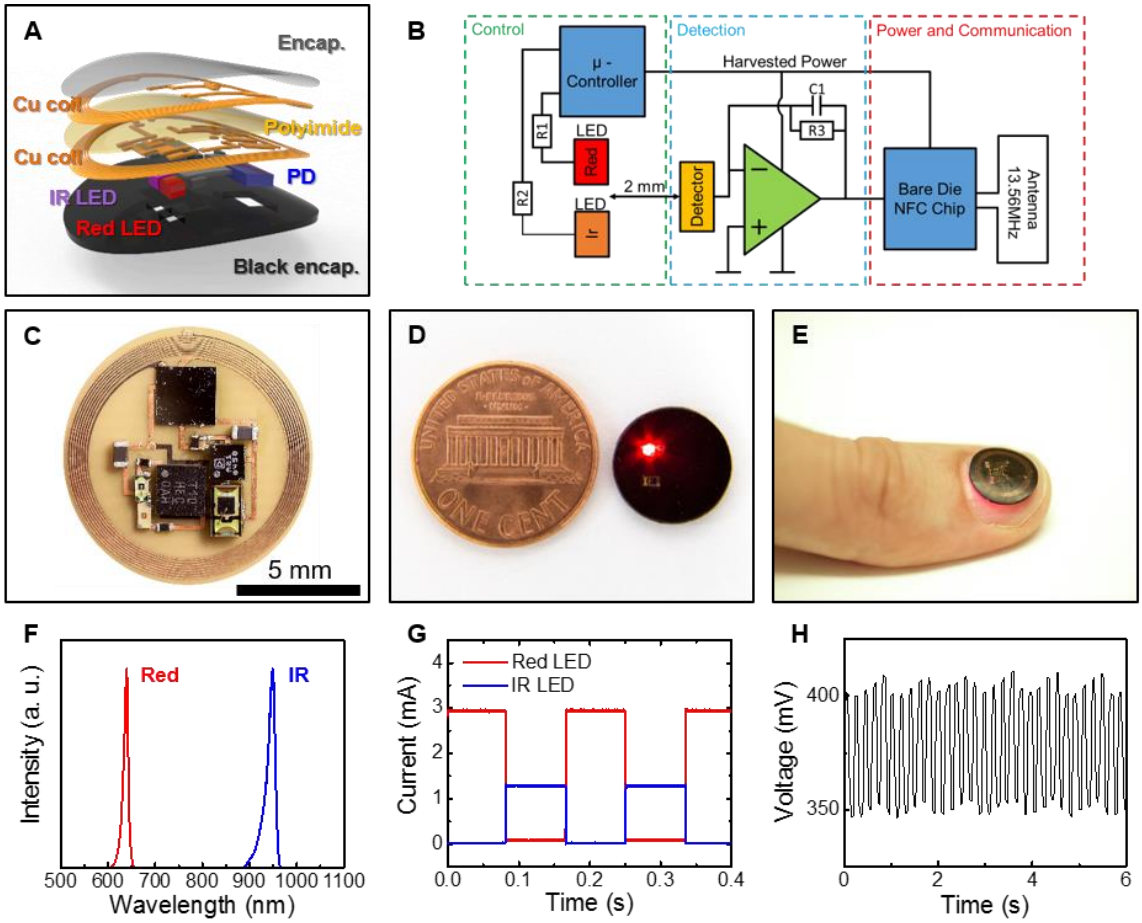
A
Encap.
Cu coil
Polyimide
Cu coil
PD
IR LED
Red LED
Black encap.
B
Control
Detection
Power and Communication
μ - Controller
Harvested Power
C1
R3
R1
LED
Red
2 mm
LED
Ir
R2
Detector
Bare Die NFC Chip
Antenna 13.56MHz
C
5 mm
D
E
F
Red
IR
Intensity (a. u.)
500 600 700 800 900 1000 1100
Wavelength (nm)
G
Red LED
IR LED
Current (mA)
0 1 2 3 4
0.0 0.1 0.2 0.3 0.4
Time (s)
H
Voltage (mV)
400
350
0 2 4 6
Time (s)

Figure 1

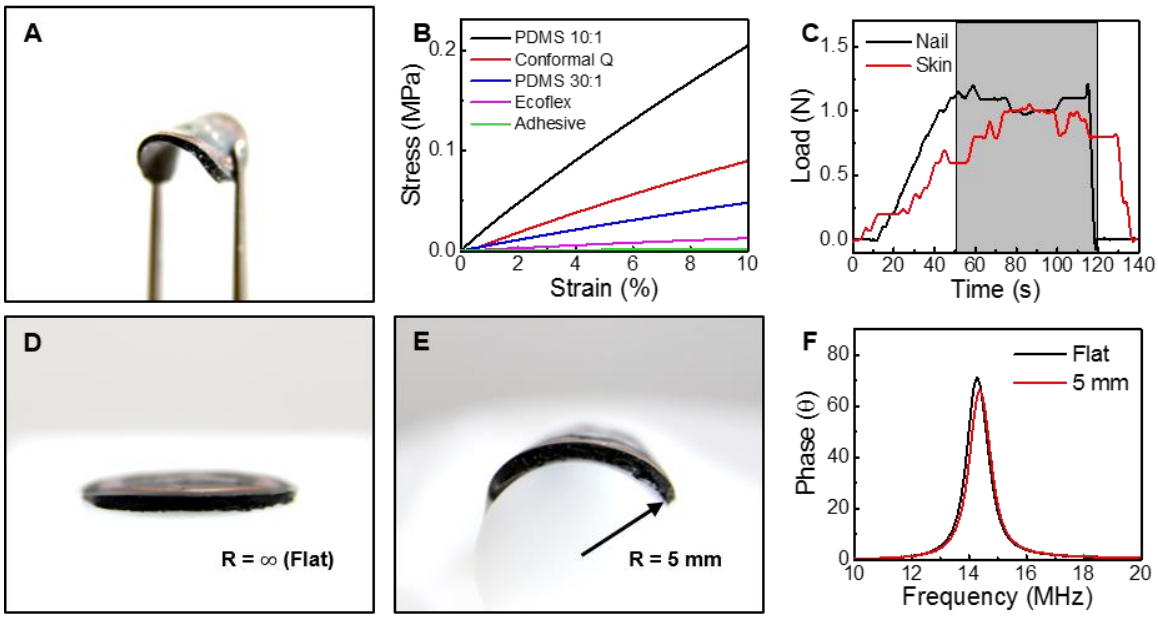
A
B
PDMS 10:1
Conformal Q
PDMS 30:1
Ecoflex
Adhesive
Stress (MPa)
Strain (%)
C
Nail
Skin
Load (N)
Time (s)
D
R = ∞ (Flat)
E
R = 5 mm
F
Flat
5 mm
Phase (θ)
Frequency (MHz)

Figure 2

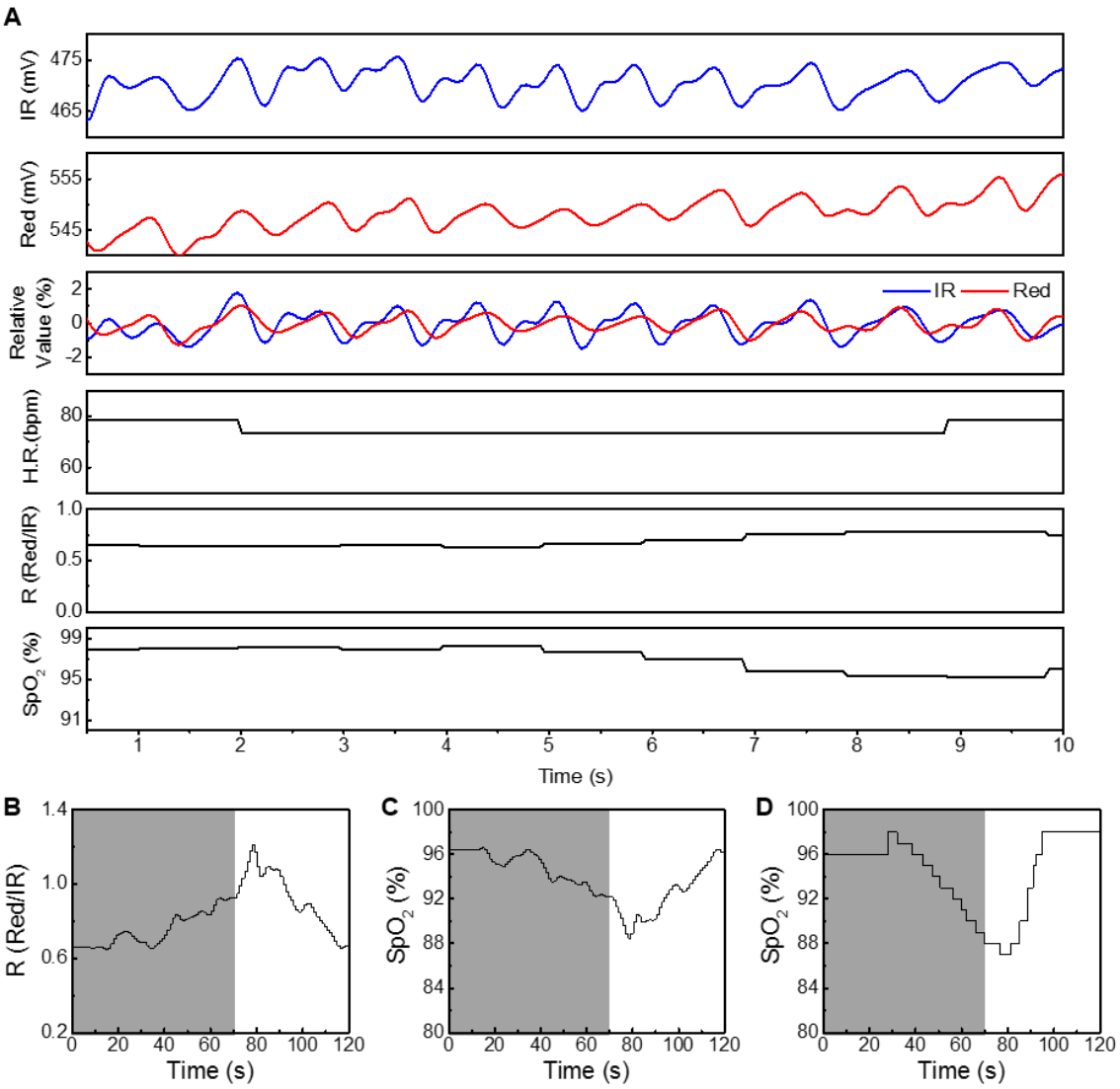
A
IR (mV)
475
465
Red (mV)
555
545
Relative Value (%)
2
0
-2
IR
Red
H.R.(bpm)
80
60
R (Red/IR)
1.0
0.5
0.0
SpO2 (%)
99
95
91
1
2
3
4
5
6
7
8
9
10
Time (s)
B
R (Red/IR)
1.4
1.0
0.6
0.2
0
20
40
60
80
100
120
Time (s)
C
SpO2 (%)
100
96
92
88
84
80
Time (s)
D
SpO2 (%)
Time (s)

Figure 3

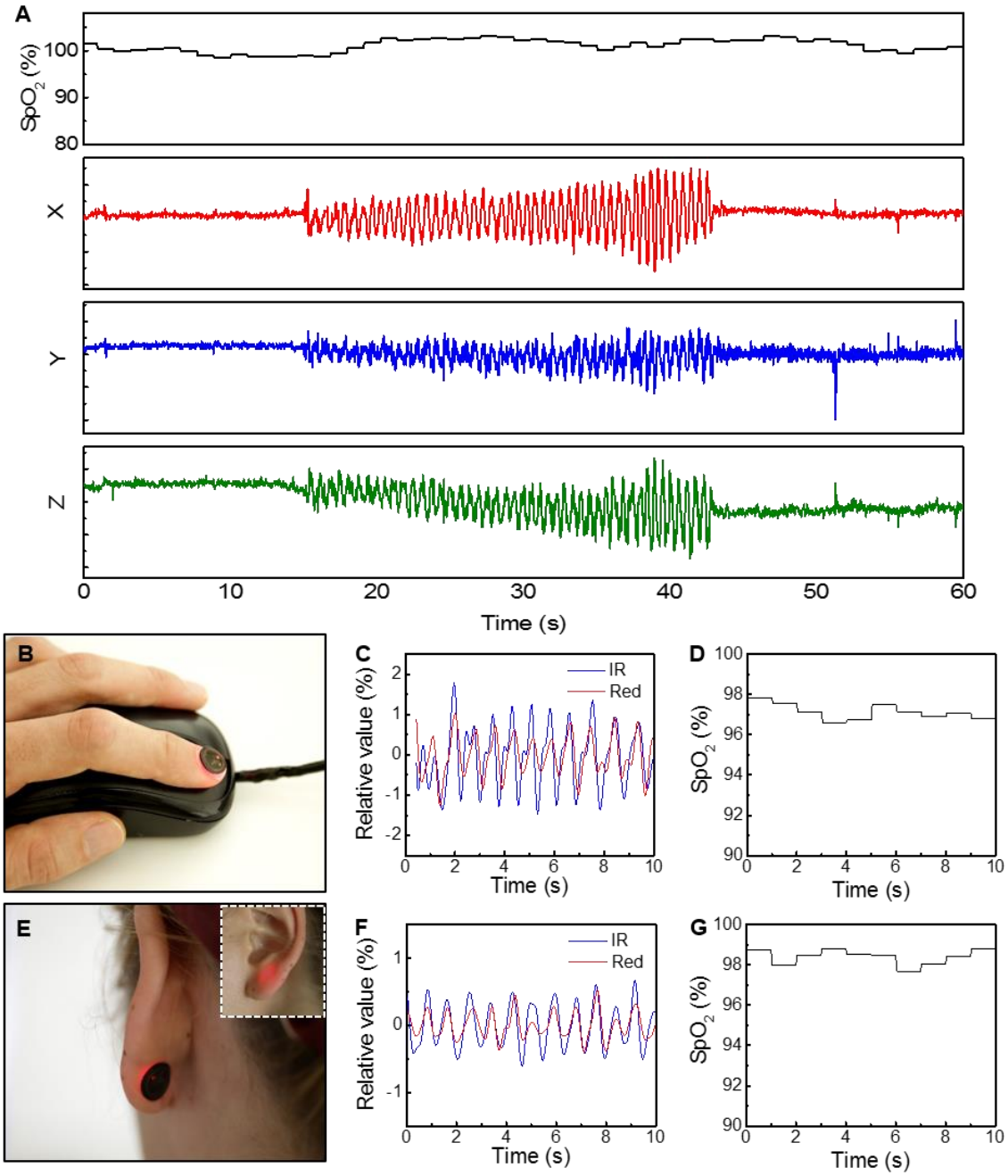
A
SpO2 (%)
100
90
80
X
Y
Z
0
10
20
30
40
50
60
Time (s)
B
C
Relative value (%)
IR
Red
Time (s)
D
SpO2 (%)
Time (s)
E
F
Relative value (%)
IR
Red
Time (s)
G
SpO2 (%)
Time (s)

Figure 4

Table 1. Mean and standard deviations of calculated SpO_2 for multiple subjects.

SpO_2	Mean (%)	STD
Subject 1	99.9	0.1
Subject 2	98.6	0.6
Subject 3	98.9	0.6
Subject 4	99.8	0.3
Subject 5	99.1	0.2
Subject 6	99.8	0.4

Table 1

The table of contents entry

We introduce materials and device concepts for ultraminiaturized wireless optoelectronic systems that incorporates advanced optoelectronic functionality for applications in wireless capture and transmission of heart rate and pulse oximetry. Specifically, reflectance pulse oximetry in conjunction with near-field communication (NFC) capabilities enable operation in thin, miniaturized flexible devices. Demonstrations of operation on various locations of the body establish the versatility and the measurement accuracy of these systems and highlight advantages of signal acquisition during operation without motion artifacts.

Keywords: NFC, oximetry, flexible electronics, wireless, photonics

*Jeonghyun Kim[†], Philipp Gutruf[†], Antonio M. Chiarelli, Seung Yun Heo, Kyoungyeon Cho, Zhaoqian Xie, Anthony Banks, Seungyoung Han, Kyung-In Jang, Jung Woo Lee, Kyu-Tae Lee, Xue Feng, Yonggang Huang, Monica Fabiani, Gabriele Gratton, Ungyu Paik, and John A. Rogers**

Miniaturized battery-free wireless pulse oximeter system

ToC figure

Supporting Video 1

Click here to access/download
Supporting Information
Video S1.mp4

Supporting Video 2

Click here to access/download
Supporting Information
Video S2.mp4

Supporting Video 3

Click here to access/download
Supporting Information
Video S3.mp4

Supporting Video 4

Click here to access/download
Supporting Information
Video S4.flv